

Model Alignment Search

Satchel Grant¹

Abstract

When can we say that two neural systems are the same? The answer to this question is goal-dependent, and it is often addressed through correlative methods such as Representational Similarity Analysis (RSA) and Centered Kernel Alignment (CKA). How do we target functionally relevant similarity, and how do we isolate specific causal aspects of the representations? In this work, we introduce Model Alignment Search (MAS), a method for causally exploring distributed representational similarity. The method learns invertible linear transformations that align a subspace between two distributed networks' representations where causal information can be freely interchanged. We first show that the method can be used to transfer values of specific causal variables—such as the number of items in a counting task—between networks with different training seeds. We then explore open questions in number cognition by comparing different types of numeric representations in models trained on structurally different tasks. We then explore differences between MAS vs preexisting causal similarity methods, and lastly, we introduce a counterfactual latent auxiliary loss function that helps shape causally relevant alignments even in cases where we do not have causal access to one of the two models for training.

1. Introduction

An important question for understanding both Artificial and Biological Neural Networks (ANNs and BNNs) is knowing what it means for one distributed system to model or represent another (Sucholutsky et al., 2023). Establishing isomorphisms between different distributed systems can be useful for simplifying their complexity and for understanding otherwise opaque inner mechanisms. We cannot yet

¹Departments of Psychology and Computer Science, Stanford University, Stanford, USA. Correspondence to: Satchel Grant <grantsrb@stanford.edu>.

Preprint under review

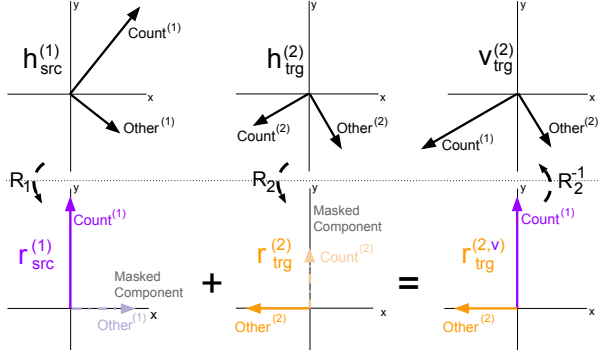


Figure 1: A theoretic causal intervention that transfers the Count information from Model₁'s latent representation, $h_{src}^{(1)}$, into Model₂'s $h_{trg}^{(2)}$. The superscripts (1) and (2) refer to the originating model. The hidden state vectors, $h_{src}^{(1)}$ and $h_{trg}^{(2)}$, are rotated into an aligned vector space using learned matrices R_1 and R_2 . In the aligned space, the Count information lies along a disentangled y axis where it can be interchanged while preserving all other information. After the transfer, the rotated, intervened vector, $r_{trg}^{(2,v)}$, is returned to Model₂'s hidden state space, using R_2^{-1} , where Model₂ can use it to continue to make predictions.

measure from every individual neuron in most BNNs; even if we could, as is the analogous case in ANNs, it is still difficult to find satisfying ways of understanding the neural behavior. Finding simplified models that exhibit the causal relationships of more complex distributed systems can make the complex systems more interpretable and communicable, potentially leading to useful insights (Cao & Yamins, 2021; 2024; Richards et al., 2019). Furthermore, there are a number of open questions about how representations differ or converge across architectures, tasks, and modalities (Huh et al., 2024; Sucholutsky et al., 2023; Wang et al., 2024; Li et al., 2024; Hosseini et al., 2024; Zhang et al., 2024).

Researchers often use correlative methods to measure the similarity of different neural representations. We can see examples of this in works that perform direct correlative analyses between ANN activations and BNN firing rates (Yamins & DiCarlo, 2016; Maheswaranathan et al., 2019), and in works that use Representational Similarity Analysis (RSA) to find 2nd order isomorphisms between model

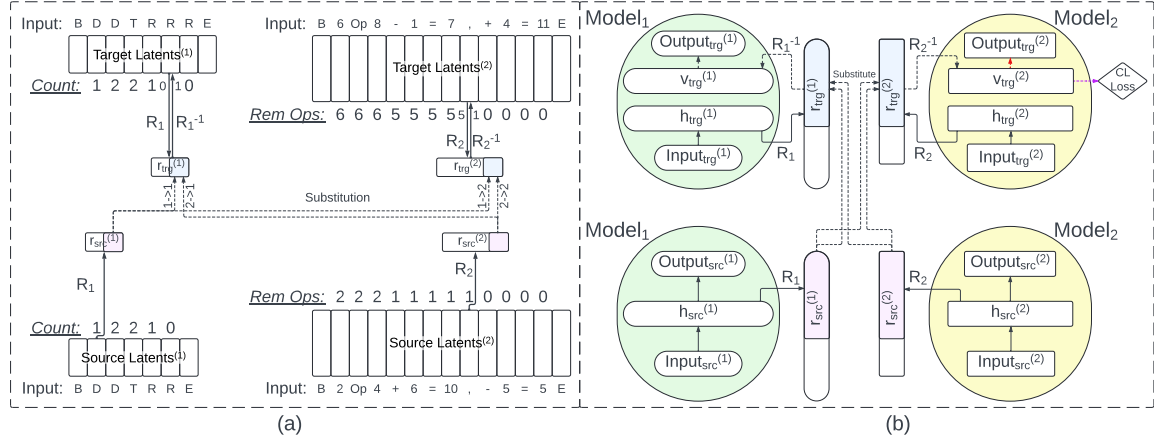


Figure 2: (a) Diagram of MAS showing all four possible intervention directions on the latent vectors (rectangles) of a Multi-Object Model₁ and an Arithmetic Model₂. The models produce the latent vectors from the input tokens. The values of the intervened causal variables—Count for the Multi-Object and Rem Ops for the Arithmetic models—are replaced by the values of the causal variables from the source. The value before the intervention is displayed on the left side of the arrows underneath the target latents, the value after the intervention is shown on the right. The dotted *Substitution* arrows correspond to a single causal intervention. After the intervention, the models make predictions using the intervened vector. Rem Ops values outside of the comma token and Count values on the B and T tokens are for visualization only. (b) Diagram of MAS and CMAS. The model weights are frozen for all models 1 and 2; the rotation matrices, R_1 and R_2 , are trained. The dashed lines indicate backpropagated gradient flow. CMAS includes gradient flow from the purple arrow extending to the Counterfactual Latent Loss (CL Loss), but does not receive gradient flow from the red arrow extending from $v_{trg}^{(2)}$. See Section 2.4 for more details.

and system (Kriegeskorte et al., 2008)—similar to Centered Kernel Alignment (Kornblith et al., 2019; Williams, 2024). We also see examples of this in linear decoding techniques, where linear decodability can be used as a metric for understanding the type of information encoded in distributed representations (Chen et al., 2020; Radford et al., 2021; Grill et al., 2020; Caron et al., 2021; Haxby et al., 2001; Haxby, 2013). A question remains, however, how to causally associate these similarity metrics with behavioral outcomes. Can we develop methods to causally understand representational alignment (Geiger et al., 2024)?

Some works have made progress toward understanding causal/functional representation similarity by transforming intermediate representations from one system into a useable state for another model. We see examples in works like *Sexton & Love (2022)* where they attempt to use transformed neural recordings in a trained computational model, and in *model stitching*, where a linear mapping is learned from intermediate representations in one ANN to another for the purpose of measuring similarity or improving one of the two models (Lähner et al., 2023; Moschella et al., 2023; Bansal et al., 2021; Lenc & Vedaldi, 2015). To build upon these works, we ask: 1) what do these causal mappings tell us about the underlying representations of the two systems? Are behaviorally successful mappings sufficient for isolating functional similarity? 2) How do we compare models

with disparate behavioral outputs, and how can we isolate the similarity of specific causal information in the representations? 3) How do we achieve causal relevance in systems that we do not have causal access?

In this work, we introduce Model Alignment Search (MAS) to measure functional distributed network similarity. MAS is a multi-model extension of Distributed Alignment Search (DAS) (Geiger et al., 2021; 2023), a technique used for aligning ANNs to symbolic algorithms (or directed acyclic graphs). MAS can be thought of as a multi-ANN extension of DAS in which MAS learns a rotation matrix for each model with the goal of finding an aligned representational subspace where information can be freely interchanged between and within the two models' aligned representations. These intervened representations are then rotated back to their original neural space which can be used to produce behavior that can be compared to expected counterfactual behavior.

We first validate MAS by comparing to similarity measurements produced by RSA in a number of modeling scenarios. We then show that MAS can reveal the representational similarity between number representations in models trained on structurally different tasks; and it can reveal representational differences between numbers used for arithmetic vs tracking cardinality. We then show that MAS is more restrictive than

previous causal methods, like direct linear mappings (model stitching), and we provide a theoretical model to better understand desired restrictions. Lastly, we provide relevance to BNNs by showing that although MAS is ineffective when one of the two models is causally inaccessible, we can introduce an auxiliary loss objective to recover causal relevance for the inaccessible model. This loss function uses *counterfactual latent* vectors—latent vectors that match the desired representational makeup of the intervened vectors assuming a successful causal intervention—as training targets for the intervened vectors of the causally inaccessible model, thus constraining the alignment to be functionally relevant for the inaccessible system. We refer to this variant as Counterfactual latent MAS (CMAS).

The contributions of this work are as follows.

1. We introduce and validate MAS by comparing and contrasting to RSA.
2. We use MAS to causally explore representations of numbers across structurally different tasks.
3. We explore how MAS can improve upon previous causal similarity methods.
4. We introduce a *counterfactual latent* auxiliary loss objective that can be used to find causally relevant alignments in cases where one of the two models is causally inaccessible (making the technique relevant for comparisons between ANNs and BNNs).

2. Methods

In this work, we build upon the work of (Grant et al., 2024) to examine the causal similarity of distributed representations within models trained on next token prediction, numeric tasks. Each model is trained to $> 99.99\%$ accuracy on both training and validation data held before being analyzed and interpreted.

2.1. Numeric Equivalence Tasks

The goal of the numeric equivalence tasks is to reproduce a quantity of tokens that is initially observed at the start of the task. Each sequence consists of two phases: the demonstration (demo) and response phases. Each sequence has an associated *object quantity* that is uniformly sampled from 1 to 20. The ordering of the demo phase consists of a Beginning of sequence token, denoted B, a number of Demonstration (D) tokens equal in quantity to the object quantity, and a Trigger (T) token. The response phase then consists of the object quantity of Response (R) tokens and ends with the End of sequence (E) token. During the model training, we include all token types in the autoregressive, cross entropy loss, even though the number of D tokens and

location of the T token is unpredictable from the sequence. A trial is considered correct when the model produces the appropriate number of R tokens followed by an E token during the response phase. We present two task variants:

Multi-Object Task: there are 3 possible demo token types $\{D_a, D_b, D_c\}$ that are uniformly sampled at each D in the sequence. There is a single response token type, R. As an example of an object quantity of 2, the sequence could be: "B D_c D_a T R R E"

Same-Object Task: there is a single token type, C, that is used as both the demo token type and the response token type. An example of an object quantity of 2 would be: "B C C T C C E".

We make a change to the Multi-Object Task when training the transformer models to prevent them from learning a solution that relies on reading out positional information (Grant et al., 2024). In this task variant, each token in the demo phase has a 0.2 probability of being sampled as a unique "void" token type, V, that is irrelevant to the completion of the numeric equivalence task. An example sequence with an object count of 2 could be: "B V D V V D T R R E". All evaluations use the original Multi-Object Task.

2.2. Arithmetic Task

We include an arithmetic task consisting of addition/subtraction operations, interlaced with the intermediate, cumulative value following each operation. An example sequence is as follows: "B 3 Op 4 + 3 = 7, + 11 = 18, - 5 = 13 E", where the numeral between B and Op indicates the number of operations in the sequence and the numeral following Op is a sampled starting value. The number of operations is uniformly sampled from 1-10. The starting value is uniformly sampled from 0-20. All numeric values are restricted to 0-20. The arithmetic operations are uniformly sampled from $\{+, -\}$ when the cumulative value is in the range 1-19. Otherwise, the operation is selected to ensure the cumulative value stays in the range 0-20. The possible operands are uniformly sampled from the set that will restrict the subsequent cumulative value to the range 0-20. The sequence then displays the cumulative value after the "=" token. The "," token indicates that there are more operations in the sequence. The sequence ends with the E token after the originally indicated number of operations. We use a base 21 token system so that all values correspond to a single token.

2.3. Model Architectures

Each model in this work is autoregressively trained to perform only one of the tasks through next-token prediction

(NTP). We train 2 model seeds for each task variant. We consider Gated Recurrent Units (GRUs) (Cho et al., 2014), Long-Short Term Memory recurrent networks (LSTMs) (Hochreiter & Schmidhuber, 1997), and two layer Transformers based on the Roformer architecture (Vaswani et al., 2017; Touvron et al., 2023; Su et al., 2023). The GRUs and Transformers use a dimensionality of 40, whereas the LSTM uses 20 dimensions for each the h and c vectors. We leave the details of GRU and LSTM cells to the referenced papers. The GRU and LSTM based models in this paper follow the structure:

$$h_{t+1} = f(h_t, x_t) \quad (1)$$

$$\hat{x}_{t+1} = g(h_{t+1}) \quad (2)$$

Where h_t is the hidden state vector at step t , x_t is the input token at step t , f is the recurrent function (either a GRU or LSTM cell), and g is a two layer (two matrix) feed-forward network (FFN) used to make a prediction, \hat{x}_{t+1} , of the token at step $t+1$ from the updated hidden state h_{t+1} .

The transformer architecture uses Rotary Positional Encodings (RoPE) (Su et al., 2023) and GELU nonlinearities (Hendrycks & Gimpel, 2023). Transformers use a history of input tokens, $X_t = [x_1, x_2, \dots, x_t]$, at each time step, t , to make a prediction: $\hat{x}_{t+1} = f(X_t)$, where f is now the transformer architecture. We show results from 2 layer, single attention head transformers. We refer readers to Figure 7 for more details. See more training details in Appendix A.1.

2.4. Model Alignment Search (MAS)

We first train the models to $> 99.99\%$ accuracy, evaluated on both training and held out validation data (we note that MAS can be used on models that are not fully trained). We freeze the model weights for the MAS analysis. MAS can be thought of as a multi-model extension of DAS (Geiger et al., 2021; 2023) where the aligned subspace is used for within model causal interventions (like in DAS) and between model interventions (similar to model stitching). We provide a visual overview in Figure 2. For each distributed system in the analysis, MAS learns an invertible transformation matrix, $\mathcal{R}_i = c_i Q_i$, composed of an orthogonal rotation matrix, $Q_i \in R^{m \times m}$, and a scaling constant, c_i . The transformation matrices rotate the models’ representations into a space where causally important information can be exchanged within and between each of the models included in the analysis. These rotation matrices are trained and evaluated using *expected counterfactual behavior* as NTP labels.

Counterfactual behavior is behavior that would have occurred if a causally important aspect of the world was different. We can see an example of this by interrupting a recurrent model’s token prediction and fully replacing its hidden representation with representations from the same model under different inputs, x , at a different time step, t . If this

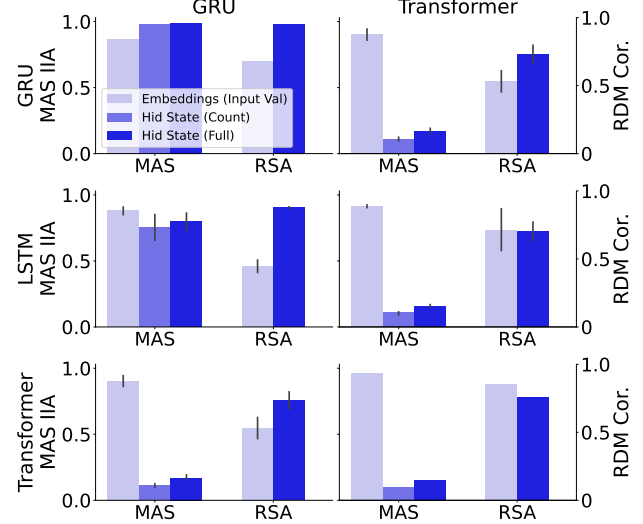


Figure 3: A performance comparison of MAS and RSA. The Model₁ architecture is consistent horizontally across panel rows. The Model₂ architecture is consistent vertically along the columns. All models are trained on the Multi-Object task. The bar colors correspond to different activation layers, and, in the case of MAS, the colors further distinguish which causal variables the analysis was conditioned upon. RDM Cor. is the value associated with an RSA whereas IIA is the intervention accuracy.

representational substitution is successful, the model will begin to produce the behavior that it had already produced under x following time step t . We refer to this behavior as the expected counterfactual behavior conditioned on a successful intervention. We can also get expected counterfactual behavior by first assuming the model implements a causal abstraction (like a computer program) and then changing the values of specific variables in this causal abstraction. i.e. transferring only the count of some number of objects while preserving all other information.

Each causal intervention attempts to transfer the value of a subspace of the rotated representation from the *source model* into a subspace of a rotated representation from the *target model* to create an intervened representation. The source and target models can be the same model. The intervened representation is then rotated back to its original space and the target model uses it to continue its predictions. We use the counterfactual behavior—the behavior that would occur if the intervention was successful and our causal abstraction is correct—as a training signal for the rotation matrices and as labels for evaluation.

Concretely, each causal intervention takes information from the *source model* and substitutes it into the *target model*. We run the source and target models on different sampled data and take a latent representation from a pre-specified

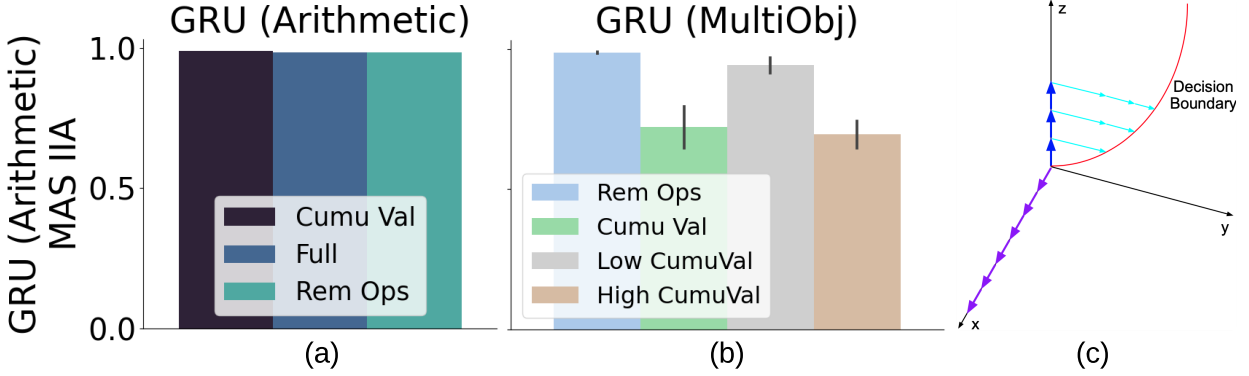


Figure 4: (a) MAS between GRUs trained on the Arithmetic task showing transferrability of the different types of information. (b) MAS used to compare the Count variable in the the Multi-Object GRUs to the Rem Ops and Cumu Val variables in the Arithmetic GRUs. Cumu Val results from MAS performed on all possible Cumu Val values. Low CumuVal results from a separate MAS analysis restricted to Cumu Val values in the range of the Rem Ops variable. High CumuVal results show a MAS analysis conditioned on values beyond the Rem Ops range. (c) Example trajectories of a theoretical model that provides a possible explanation for why Linear Map results can be inflated relative to MAS. See Section 3.4 for more details.

layer for each model from some uniformly sampled time step t for the target model and time u for the source model. These hidden representations are denoted as $h_{trg,t}^{(i)} \in R^{m_i}$ and $h_{src,u}^{(j)} \in R^{m_j}$ for the target and source models respectively, where m_k is the number of neurons in the distributed representation from model k . In Figure 2 we can see all four directional permutations for the two models. In the figure, the time step of the latent is abstracted away, and $h^{(k)}$ is labeled as $h_{\phi}^{(k)}$ where k is the model index and $\phi \in \{trg, src\}$ denotes when f_k is the target model or source model.

To perform the causal intervention, we rotate $h_{trg,t}^{(i)}$ and $h_{src,u}^{(j)}$ using the corresponding matrices \mathcal{R}_i and \mathcal{R}_j into the transformed representations $r_{trg,t}^{(i)}$ and $r_{trg,u}^{(j)}$. We then replace a learned or predefined number of dimensions in the target vector $r_{trg,t}^{(i)}$ with the values from the same dimensions from the source vector $r_{src,u}^{(j)}$ to create a new, intervened representation $r_{trg,t}^{(i,v)}$. The substituted dimensions are colored in the $r_{\phi}^{(k)}$ vectors in the diagram with the label "Aligned." Lastly, we return $r_{trg,t}^{(i,v)}$ to the original representation space of i using the inverse of the transformation \mathcal{R}_i to create $v_{trg,t}^{(i)}$. A single causal intervention on two $h^{(k)}$ vectors can be written as:

$$v_{trg,t}^{(i)} = \mathcal{R}_i^{-1}((1 - D_i)\mathcal{R}_i h_{trg,t}^{(i)} + D_j \mathcal{R}_j h_{src,u}^{(j)}) \quad (3)$$

Where $D_i \in R^{m_i \times m_i}$ and $D_j \in R^{m_j \times m_j}$ are diagonal, binary matrices with the same non-zero entries along the diagonal. The non-zero values are organized contiguously along the diagonal starting from the upper left index, $(0,0)$. These matrices are used to isolate the desired number of dimensions to replace in $r_{trg,t}^{(i)}$. We refer to the space spanned

by $D_k r^{(k)}$ as the aligned subspace of the models' representations. This is where the causally relevant information can be freely exchanged. We can handle cases where $m_i \neq m_j$ by setting the number of non-zero entries in both D_k to be $\min(m_i, m_j)$. The binary values along the diagonal of D can be learned or pre-specified (Geiger et al., 2023). In this work, all experiments pre-specify the number of dimensions to be half of the smallest m_k unless otherwise noted. The last step in the process is to allow the target model, $f_{trg,i}$, to continue making predictions using $v_{trg,t}^{(i)}$ as its hidden state. We simply discard $h_{src,u}^{(j)}$ and $h_{trg,t}^{(i)}$.

We train the transformation matrices, \mathcal{R}_i and \mathcal{R}_j , using the gradient signal generated from an autoregressive cross entropy loss on the counterfactual sequences. Once we have trained the rotation matrices to convergence, we can evaluate the quality of the model alignment using the accuracy of each model's predictions on the expected counterfactual behavior of unseen causal interventions. This accuracy is referred to as the Interchange Intervention Accuracy (IIA). Higher IIAs indicate stronger alignments between the models used in the analysis. We report the minimum performance of the four possible intervention directions. See more training details in Appendix A.2.

2.5. Full vs Specific Variable MAS

The choice of the counterfactual behavior defines what variable(s) MAS attempts to find an aligned subspace for. We have the option to align all behaviorally relevant information by simply using the exact behavior of the source model as the counterfactual behavior. This is similar to model stitching in previous works such as Bansal et al. (2021); Lenc & Vedaldi (2015); Sexton & Love (2022). In these

cases of complete information transfer, MAS still differs from previous works in that it 1. performs the interventions in multiple causal directions within a single analysis and 2. it can align a functional subspace of the activations rather than the complete latent space. MAS also can target a specific type of information for transfer by conditioning the counterfactual sequences on a specific causal variable (i.e. the count of the sequence). In all numeric equivalence tasks, we prevent interventions on representations resulting from the BOS, T, and EOS tokens. In the arithmetic task, we only perform interventions on representations after the “,” token. We perform MAS using each of the following causal variables, where the corresponding task is denoted in parentheses:

1. **Full** (Arithmetic/Num Equivalence): Refers to cases in which we transfer all causally relevant information between models (not all activations).
2. **Count** (Num Equivalence): The difference between the number of observed demo tokens and the number of response tokens in the sequence. Example: the following sequences have a Count of 2 at the last token: “B D D” ; “B D D D T R”
3. **Last Value** (Num Equivalence): The value of the input token with respect to changing the Count of the sequence. We assign the values as D=1, R=-1, and all other tokens are 0. Example: if we change the Last Value of a single D token from 1 to -1, the counterfactual sequence should be “B D D D T R E”. Example: in a partial sequence “B D D T R”, changing the R token from -1 to 1 results in: “B D D T R R R E”.
4. **Cumu Val** (Arithmetic): The cumulative value of the arithmetic sequence in the Arithmetic task. Example: if we substitute in a value of 3 at the “,” token in the sequence “B 2 Op 3 + 5 = 8 ,” the counterfactual sequence could be “B 2 Op 3 + 5 = 8 , + 2 = 5 E” where the “+” and “2” are provided by the task.
5. **Rem Ops** (Arithmetic): The remaining number of operations in the arithmetic sequence. Example: we substitute in a value of 1 at the “,” token in the sequence “B 3 Op 3 + 5 = 8 ,” the counterfactual sequence could be “B 3 Op 3 + 5 = 8 , + 1 = 9 E” where the “+” and “1” are provided.

2.6. Additional Methods

Representational Similarity Analysis (RSA): For a given model layer, we run the model on a batch of sequences consisting of 15 sequences from each object quantity 1-20. We then sample 1000 representational vectors uniformly from all time points excluding padding and end of sequence tokens. We construct a Representational Dissimilarity Matrix

(RDM) as 1 minus the cosine similarity matrix over each pair-wise comparison of the representations (resulting in an RDM of dimensions 1000×1000). We create an RDM for two models and compare the RDMs using Spearman’s rank correlation on the lower triangle of each matrix (Virtanen et al., 2020). We perform the RDM sampling 10 times and report the average over all 10 correlations. See more details in Appendix A.3.

Unidirectional MAS (UniMAS): MAS described up to this point systematically runs training batches of all index pairings $(i, j) \in \{(1, 1), (1, 2), (2, 1), (2, 2)\}$ for two models $f_1(h, x)$ and $f_2(h, x)$. In some settings, however, we wish to compare to models for which we have neural recordings but no causal access to the model (as is often the case in BNNs). UniMAS uses the activations from both models as source activations, but only uses f_1 as the target model for MAS trainings. Concretely, we train both rotation matrices without backpropagating gradient information from the counterfactual predictions of the *causally inaccessible model*, f_2 . As a baseline, we include **Linear Maps** which are trainings that exclusively use model 2 as the source model and model 1 as the target model. In Full variable settings, we transfer the complete rotated vector between models.

Counterfactual latent MAS (CMAS): The UniMAS trainings fail to learn an R_2 with strong IIA in the inaccessible model. To address this, we introduce an auxiliary loss function to the UniMAS trainings. The auxiliary objective relies on *Counterfactual Latent (CL) vectors*. We define CL vectors as latent vectors that encode the causal variables that we would expect to exist in the intervened vector, $v_{trg, t}^{(2)}$ from Equation 3, after a successful causal intervention. We obtain these CL vectors from a neural representation dataset possessing situations and behaviors that are consistent with the information we wish to be encoded after the causal intervention. Concretely, if we expect $v_{trg, t}^{(2)}$ to have a Count of 2 in the demo phase after the intervention, the CL vector could be obtained from the representation following the underlined D in the sequence “B D D T R R E”. The auxil-

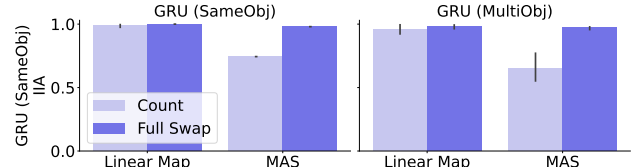


Figure 5: Performance comparison of MAS and direct linear mappings (Linear Map) between the Same-Object GRUs and between the Same-Object and Multi-Object GRUs. The Count information can be successfully transferred to and from Same-Object GRUs when using Linear Map but not in MAS.

iary objective applies an L2 loss and a cosine loss using CL vectors as the ground truth.

Relabeling $v_{trg,t}^{(2)}$ as v and denoting the CL vector as $h^{(c)}$, we calculate the auxiliary loss, \mathcal{X} , for a single batch of interventions as the following:

$$\mathcal{X} = \frac{1}{N} \sum_k^N \left(\frac{1}{2} \|v_k - h_k^{(c)}\|_2^2 - \frac{1}{2} \frac{v_k \cdot h_k^{(c)}}{\|v_k\|_2 \|h_k^{(c)}\|_2} \right) \quad (4)$$

where k denotes the index of the sample within the batch. The total CMAS training loss, \mathcal{L} , is a weighted average of the UniMAS autoregressive loss, denoted \mathcal{U} , and the auxiliary loss. $\mathcal{L} = \lambda \mathcal{X} + (1 - \lambda) \mathcal{U}$ where λ is a tunable hyperparameter. As a baseline we include **Latent Fit** trainings that directly map latent representations from one model to another under the same inputs without a behavioral training objective, only using the MSE, cosine loss, or both latent objectives from model 1 to model 2's latent vectors. We report the transform with the best IIA.

3. Results/Discussion

3.1. MAS

We first turn our attention to the MAS IIA in Figure 3. The figure shows analyses where Model₁ is consistent horizontally across each row and Model₂ is displayed vertically along each column. We exclude comparisons of each model seed with itself. We see the MAS results conditioned on three different variables: Full, Count, and Last Value (see Section 2.5). The IIA shows the proportion of trials with successful counterfactual behavior after the causal interventions. A trial is considered successful if all deterministic counterfactual tokens are predicted correctly. For the Full and Count variables, causal interventions are performed on the hidden state vector after the recurrent processing in recurrent models and on the hidden states following the first transformer layer in transformers. Causal interventions conditioned on the Last Value variable are performed on the input embedding layer in all architectures.

We see from Figure 3 and Appendix 8 that MAS is successful at performing the Full variable interventions between different recurrent model seeds. This is consistent with the findings of previous work on direct linear mappings between networks (Lenc & Vedaldi, 2015; Bansal et al., 2021; Lähner et al., 2023; Sexton & Love, 2022; Sucholutsky et al., 2023). Furthermore, MAS is successful at transferring the Count between the Multi-Object GRUs that have previously been shown to have an interchangeable Count variable using DAS (Grant et al., 2024). This success is qualified by MAS' inability to transfer the Count when one of the two models is a Same-Object GRU (Figure 5), which is also expected from DAS. MAS on the hidden states of the transformers is largely unsuccessful with a value of 0.087, whereas MAS on

the embeddings is successful with a value of 0.961. This is consistent with previous work that has shown the transformers solve the numeric equivalence tasks without encoding a Markovian cumulative state. Instead, they rely on re-solving the task at each step in the sequence (Grant et al., 2024; Behrens et al., 2024). See Figure 8 for DAS results.

3.2. MAS vs RSA

RSA is a second order correlational method that examines the similarity between sample correlation matrices constructed from two models' representations (see Appendix A.3 for details). We provide comparisons between models differing only by seed to establish an upper limit on MAS and RSA values. We also provide GRU-LSTM comparisons to establish value changes resulting from architectural differences. Turning to Figure 3 and Appendix 8, we highlight that RSA provides a lower value than MAS on the embedding layers and a larger value than MAS on the hidden states of the transformers. In the case of the hidden states in the Transformer-Transformer comparison (the lower rightmost panel), we see an RSA value of 0.78 and a CKA value of 0.96 in the appendix. The values in this comparison are difficult to interpret, as we might expect higher values due to similarities in architecture and training, but we also know from causal experiments that there is little causal transferrability between the transformers' representations. We note that questions on how to interpret RSA values have been addressed in previous works (Kriegeskorte et al., 2008; Sucholutsky et al., 2023; Dujmović et al., 2022).

3.3. Arithmetic

We include a MAS analysis between Arithmetic GRUs and GRUs trained on the Numeric Equivalence tasks (see Figure 4). The leftmost panel shows that we can successfully align the Cumu Val, and the Rem Ops variables between and within the Arithmetic GRUs. The middle panel shows that MAS can successfully align the Count with the Rem Ops variables between GRUs trained on the Multi-Object and Arithmetic tasks respectively. These results are qualified by the lower IIA alignment between the Count and the Cumu Val variables. We see that when we perform MAS only on Cumu Val values that are shared with possible the Rem Ops values (Low CumuVal), the results are much higher but still do not match the results from Rem Ops. These findings are consistent with the hypothesis that these GRUs are using different types of numeric representations for arithmetic than incremental counting.

3.4. Direct Linear Mappings

Turning to Figure 5, we compare the IIA of MAS to direct linear mappings (denoted Linear Map). The Linear Map trainings are equivalent to MAS trained in a single causal

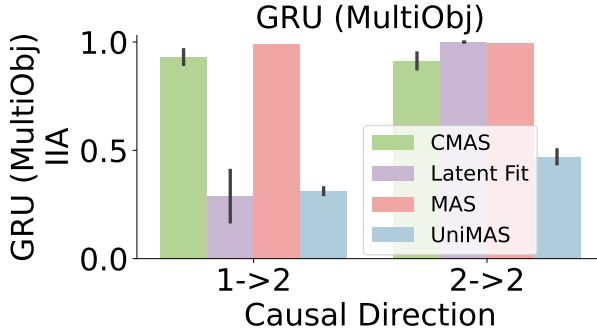


Figure 6: The IIAs in the causally untrained directions for CMAS on the Multi-Object GRU models on the Full variable. The x labels denote the intervention directions where “1” and “2” denote the model index and the arrow points from the source to the target model. Latent Fit variants fit a transformation to the latent vectors in one direction without including causal behavior training. UniMAS and MAS show a lower and upper bound on CMAS performance. The $2 \rightarrow 2$ Latent Fit direction is trivial.

direction with the IIA reported from only that trained causal direction. We see that the Count variable can be successfully transferred between the Same-Object GRUs when using direct linear mappings. This is in contrast to MAS and the results of DAS from previous work (Grant et al., 2024). We introduce a theoretical model in Figure 4 as a possible explanation.

Turning to Figure 4, we see three components of a theoretical models’ state vector and their corresponding values at different points along 3 different trajectories. Each trajectory begins at the 0,0,0 coordinate. Each dark blue arrow represents an increment in the number of demo tokens, allowing the total number of demo tokens to be represented as the magnitude of the z-component. The number of response tokens is encoded along the y-axis, and the red curve represents the model’s decision boundary for outputting the E token. For a single trajectory, this model effectively counts up along the z-axis, then counts along the y-axis, and finishes when it has reached the non-linear decision boundary. Along the x-axis, we show a vector component that does not affect the model’s functional solution to the task, but still encodes relevant information. In this model, it is possible to linearly decode the Count using the difference between twice the magnitude of the z-component and the magnitude of the x-component. More precisely, $\text{Count} = 2z - x$. It is possible to then map this information to the equivalent of the z-axis in a similar target model while discarding its y-component. This target model could then continue counting demo tokens or begin counting response tokens depending on its phase. It is important to note that this substitution is likely only possible if the mapping can push all conflict-

ing causally relevant information into the null space of the target model; remnants of the z or y components could interfere with the counterfactual behavior. This effect is only a potential explanation for why the IIA observed in MAS is lower. Namely, the within model MAS interventions could prevent solutions that “throw away” residual information. We do not make efforts to prove that this theoretical model accounts for the results we see in Figure 5, it only serves as a *potential* explanation for the results.

3.5. CMAS

We can see from Figure 6 the results of CMAS compared to MAS, UniMAS, and Latent Fits. It is important to note that the Latent Fit, UniMAS, and CMAS variants do not include the autoregressive counterfactual training signal in causal directions $1 \rightarrow 2$ and $2 \rightarrow 2$. MAS provides a theoretic upper bound on the possible IIA for CMAS. UniMAS provides a lower bound on the possible CMAS performance. We also note that the UniMAS results demonstrate that the causally relevant \mathcal{R}_2^{-1} is not automatically learned. Lastly, Latent Fit—which trains a rotation matrix to map latent vectors from Model₁ to latent vectors of Model₂ without any causal behavioral training—provides a baseline of existing methods. We see that CMAS recovers much of the possible performance of MAS whereas the Latent Fit performs near the lower bound. This demonstrates the potential of CMAS to recover causally relevant intervention rotation matrices even when we do not have causal access to one of the models in the comparison.

4. Limitations/Future Directions

We highlight that our results demonstrate the possibility to learn alignments that are functionally relevant in only one causal direction. Although MAS does not guarantee isolation and alignment of only functionally relevant information, it is more restrictive than existing methods while allowing for the desired alignment of functional information. Future MAS explorations can narrow the focus on functional information by finding the minimum transferrable subspace.

Despite CMAS’s successes, we are aware of the difficulty of evaluating the causal relevance of the interventions without causal access to the inaccessible model. We note, however, that CMAS still may provide value in biological settings as the method can potentially remove the need for BNN counterfactual behavioral training data by using a brute-force approach of multiple independent CMAS trainings that can then be evaluated for causal relevance.

Acknowledgments

Thank you to the PDP Lab and the Stanford Psychology department for funding. Thank you to Stephen Baccus,

Noah Goodman, Zen Wu, Atticus Geiger, Linas Nasvytis, Jenelle Feather, Chris Potts, Alexa Tartaglini, Daniel Wuragaft, the PDP lab, and the Stanford Mech Interp community for thoughtful discussion. Thanks to Joshua Melander, Josh Wilson, Ben Prystawski, Jerome Han, and Andrew Lampinen for thoughtful discussion and paper feedback. Special thanks to Jay McClelland for encouragement, paper feedback, and many thoughtful conversations.

Impact Statement

This paper presents work whose goal is to advance the field of Machine Learning, Cognitive Science, and Systems Neuroscience. There are many potential societal consequences of this work, none which we feel must be specifically highlighted here.

References

- Ba, J. L., Kiros, J. R., and Hinton, G. E. Layer normalization, 2016. URL <https://arxiv.org/abs/1607.06450>.
- Bansal, Y., Nakkiran, P., and Barak, B. Revisiting Model Stitching to Compare Neural Representations, June 2021. URL <https://arxiv.org/abs/2106.07682>. arXiv:2106.07682 [cs, stat].
- Behrens, F., Biggio, L., and Zdeborová, L. Counting in small transformers: The delicate interplay between attention and feed-forward layers, 2024. URL <https://arxiv.org/abs/2407.11542>.
- Cao, R. and Yamins, D. Explanatory models in neuroscience: Part 1 – taking mechanistic abstraction seriously, April 2021. URL <https://arxiv.org/abs/2104.01490>. arXiv:2104.01490 [cs, q-bio].
- Cao, R. and Yamins, D. Explanatory models in neuroscience, Part 2: Functional intelligibility and the contravariance principle. *Cognitive Systems Research*, 85:101200, June 2024. ISSN 1389-0417. doi: 10.1016/j.cogsys.2023.101200. URL <https://www.sciencedirect.com/science/article/pii/S1389041723001341>.
- Caron, M., Touvron, H., Misra, I., Jégou, H., Mairal, J., Bojanowski, P., and Joulin, A. Emerging properties in self-supervised vision transformers, 2021.
- Chen, T., Kornblith, S., Norouzi, M., and Hinton, G. A simple framework for contrastive learning of visual representations. 2020.
- Cho, K., van Merriënboer, B., Gülcühre, Ç., Bougares, F., Schwenk, H., and Bengio, Y. Learning phrase representations using RNN encoder-decoder for statistical machine translation. *CoRR*, abs/1406.1078, 2014. URL <http://arxiv.org/abs/1406.1078>.
- Dujmović, M., Bowers, J. S., Adolfi, F., and Malhotra, G. The pitfalls of measuring representational similarity using representational similarity analysis. *bioRxiv*, 2022. doi: 10.1101/2022.04.05.487135. URL <https://www.biorxiv.org/content/early/2022/04/07/2022.04.05.487135>.
- Geiger, A., Lu, H., Icard, T., and Potts, C. Causal abstractions of neural networks. *CoRR*, abs/2106.02997, 2021. URL <https://arxiv.org/abs/2106.02997>.
- Geiger, A., Wu, Z., Potts, C., Icard, T., and Goodman, N. D. Finding alignments between interpretable causal variables and distributed neural representations, 2023.
- Geiger, A., Ibeling, D., Zur, A., Chaudhary, M., Chauhan, S., Huang, J., Arora, A., Wu, Z., Goodman, N., Potts, C., and Icard, T. Causal abstraction: A theoretical foundation for mechanistic interpretability, 2024. URL <https://arxiv.org/abs/2301.04709>.
- Grant, S., Goodman, N. D., and McClelland, J. L. Emergent symbol-like number variables in artificial neural networks, 2024.
- Grill, J.-B., Strub, F., Altché, F., Tallec, C., Richemond, P. H., Buchatskaya, E., Doersch, C., Pires, B. A., Guo, Z. D., Azar, M. G., Piot, B., Kavukcuoglu, K., Munos, R., and Valko, M. Bootstrap your own latent: A new approach to self-supervised learning, 2020.
- Haxby, J. V. Multivariate pattern analysis of fMRI: Parcellating abstract from concrete representations. *NEuroimage*, 62(2):2013, 2013. doi: 10.1016/j.neuroimage.2012.03.016. Multivariate.
- Haxby, J. V., Gobbini, M. I., Furey, M. L., Ishai, A., Schouten, J. L., and Pietrini, P. Distributed and overlapping representations of faces and objects in ventral temporal cortex. *Social Neuroscience: Key Readings*, 293 (September):87–96, 2001. doi: 10.4324/9780203496190.
- Hendrycks, D. and Gimpel, K. Gaussian error linear units (gelus), 2023. URL <https://arxiv.org/abs/1606.08415>.
- Hochreiter, S. and Schmidhuber, J. Long short-term memory. *Neural Comput.*, 9(8):1735–1780, nov 1997. ISSN 0899-7667. doi: 10.1162/neco.1997.9.8.1735. URL <https://doi.org/10.1162/neco.1997.9.8.1735>.
- Hosseini, E., Casto, C., Zaslavsky, N., Conwell, C., Richardson, M., and Fedorenko, E. Universality of representation in biological and artificial neural networks. *bioRxiv*, 2024. doi: 10.1101/2024.12.26.629294.

- URL <https://www.biorxiv.org/content/early/2024/12/26/2024.12.26.629294>.
- Huh, M., Cheung, B., Wang, T., and Isola, P. The platonic representation hypothesis, 2024. URL <https://arxiv.org/abs/2405.07987>.
- Kornblith, S., Norouzi, M., Lee, H., and Hinton, G. Similarity of neural network representations revisited, 2019. URL <https://arxiv.org/abs/1905.00414>.
- Kriegeskorte, N., Mur, M., and Bandettini, P. Representational similarity analysis - connecting the branches of systems neuroscience. *Frontiers in Systems Neuroscience*, 2, 2008. ISSN 1662-5137. doi: 10.3389/neuro.06.004.2008. URL <https://www.frontiersin.org/articles/10.3389/neuro.06.004.2008>.
- Lenc, K. and Vedaldi, A. Understanding image representations by measuring their equivariance and equivalence, 2015. URL <https://arxiv.org/abs/1411.5908>.
- Li, J., Kementchedjhieva, Y., Fierro, C., and Søgaard, A. Do Vision and Language Models Share Concepts? A Vector Space Alignment Study. *Transactions of the Association for Computational Linguistics*, 12:1232–1249, September 2024. ISSN 2307-387X. doi: 10.1162/tacl_a_00698. URL https://doi.org/10.1162/tacl_a_00698.
- Lähner, Z., Moeller, M., Fumero, M., Rodolà, E., Domine, C., Locatello, F., Dziugaite, K., and Caron, M. On the Direct Alignment of Latent Spaces. 2023.
- Maheswaranathan, N., McIntosh, L. T., Tanaka, H., Grant, S., Kastner, D. B., Melander, J. B., Nayebi, A., Brezovec, L., Wang, J., Ganguli, S., and Baccus, S. A. The dynamic neural code of the retina for natural scenes. *bioRxiv*, 2019. doi: 10.1101/340943. URL <https://www.biorxiv.org/content/early/2019/12/17/340943>.
- Moschella, L., Maiorca, V., Fumero, M., Norelli, A., Locatello, F., and Rodolà, E. Relative representations enable zero-shot latent space communication, March 2023. URL <http://arxiv.org/abs/2209.15430>. arXiv:2209.15430 [cs].
- Paszke, A., Gross, S., Massa, F., Lerer, A., Bradbury, J., Chanan, G., Killeen, T., Lin, Z., Gimelshein, N., Antiga, L., Desmaison, A., Köpf, A., Yang, E. Z., DeVito, Z., Raison, M., Tejani, A., Chilamkurthy, S., Steiner, B., Fang, L., Bai, J., and Chintala, S. Pytorch: An imperative style, high-performance deep learning library. *CoRR*, abs/1912.01703, 2019. URL <http://arxiv.org/abs/1912.01703>.
- Radford, A., Kim, J. W., Hallacy, C., Ramesh, A., Goh, G., Agarwal, S., Sastry, G., Askell, A., Mishkin, P., Clark, J., Krueger, G., and Sutskever, I. Learning transferable visual models from natural language supervision, 2021.
- Richards, B. A., Lillicrap, T. P., Beaudoin, P., Bengio, Y., Bogacz, R., Christensen, A., Clopath, C., Costa, R. P., de Berker, A., Ganguli, S., Gillon, C. J., Hafner, D., Kepecs, A., Kriegeskorte, N., Latham, P., Lindsay, G. W., Miller, K. D., Naud, R., Pack, C. C., Poirazi, P., Roelfsema, P., Sacramento, J., Saxe, A., Scellier, B., Schapiro, A. C., Senn, W., Wayne, G., Yamins, D., Zenke, F., Zylberberg, J., Therien, D., and Kording, K. P. A deep learning framework for neuroscience. *Nature Neuroscience*, 22(11):1761–1770, November 2019. ISSN 1546-1726. doi: 10.1038/s41593-019-0520-2. URL <https://www.nature.com/articles/s41593-019-0520-2>. Publisher: Nature Publishing Group.
- Sexton, N. J. and Love, B. C. Reassessing hierarchical correspondences between brain and deep networks through direct interface. *Science Advances*, 8(28):eabm2219, July 2022. doi: 10.1126/sciadv.abm2219. URL <https://www.science.org/doi/10.1126/sciadv.abm2219>. Publisher: American Association for the Advancement of Science.
- Su, J., Lu, Y., Pan, S., Murtadha, A., Wen, B., and Liu, Y. Roformer: Enhanced transformer with rotary position embedding, 2023.
- Sucholutsky, I., Muttenthaler, L., Weller, A., Peng, A., Bobu, A., Kim, B., Love, B. C., Grant, E., Groen, I., Achterberg, J., Tenenbaum, J. B., Collins, K. M., Hermann, K. L., Oktar, K., Greff, K., Hebart, M. N., Jacoby, N., Zhang, Q., Marjeh, R., Geirhos, R., Chen, S., Kornblith, S., Rane, S., Konkle, T., O’Connell, T. P., Unterthiner, T., Lampinen, A. K., Müller, K.-R., Toneva, M., and Griffiths, T. L. Getting aligned on representational alignment, 2023. URL <https://arxiv.org/abs/2310.13018>.
- Touvron, H., Lavril, T., Izacard, G., Martinet, X., Lachaux, M.-A., Lacroix, T., Rozière, B., Goyal, N., Hambro, E., Azhar, F., Rodriguez, A., Joulin, A., Grave, E., and Lample, G. Llama: Open and efficient foundation language models, 2023.
- Vaswani, A., Shazeer, N., Parmar, N., Uszkoreit, J., Jones, L., Gomez, A. N., Kaiser, L., and Polosukhin, I. Attention is all you need. *CoRR*, abs/1706.03762, 2017. URL <http://arxiv.org/abs/1706.03762>.
- Virtanen, P., Gommers, R., Oliphant, T. E., Haberland, M., Reddy, T., Cournapeau, D., Burovski, E., Peterson, P., Weckesser, W., Bright, J., van der Walt, S. J., Brett, M., Wilson, J., Millman, K. J., Mayorov, N., Nelson, A. R. J.,

Jones, E., Kern, R., Larson, E., Carey, C. J., Polat, İ., Feng, Y., Moore, E. W., VanderPlas, J., Laxalde, D., Perktold, J., Cimrman, R., Henriksen, I., Quintero, E. A., Harris, C. R., Archibald, A. M., Ribeiro, A. H., Pedregosa, F., van Mulbregt, P., and SciPy 1.0 Contributors. SciPy 1.0: Fundamental Algorithms for Scientific Computing in Python. *Nature Methods*, 17:261–272, 2020. doi: 10.1038/s41592-019-0686-2.

Wang, J., Ge, X., Shu, W., Tang, Q., Zhou, Y., He, Z., and Qiu, X. Towards Universality: Studying Mechanistic Similarity Across Language Model Architectures, October 2024. URL <http://arxiv.org/abs/2410.06672>. arXiv:2410.06672 [cs].

Williams, A. H. Equivalence between representational similarity analysis, centered kernel alignment, and canonical correlations analysis. *bioRxiv*, 2024. doi: 10.1101/2024.10.23.619871. URL <https://www.biorxiv.org/content/early/2024/10/24/2024.10.23.619871>.

Yamins, D. L. and DiCarlo, J. J. Using goal-driven deep learning models to understand sensory cortex. *Nature Neuroscience*, 19(3):356–365, 2016. ISSN 15461726. doi: 10.1038/nn.4244.

Zar, J. H. Spearman rank correlation. *Encyclopedia of Biostatistics*, 7, 2005.

Zhang, L., Yang, Q., and Agrawal, A. Assessing and learning alignment of unimodal vision and language models, 2024. URL <https://arxiv.org/abs/2412.04616>.

A. Appendix / Supplementary material

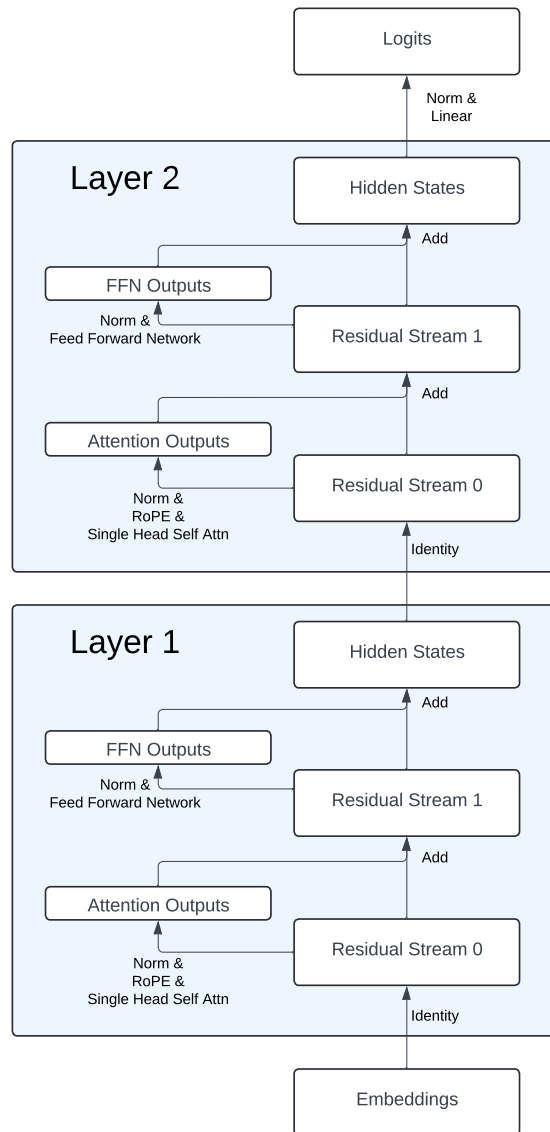


Figure 7: Figure and caption taken from Grant et al. (2024). Diagram of the transformer architecture used in this work. White rectangles represent activation vectors, arrows represent functional operations. All causal interventions were performed on either the Hidden State activations from Layer 1 or the Embeddings layer. All normalizations are Layer Norms (Ba et al., 2016).

Model Alignment Search

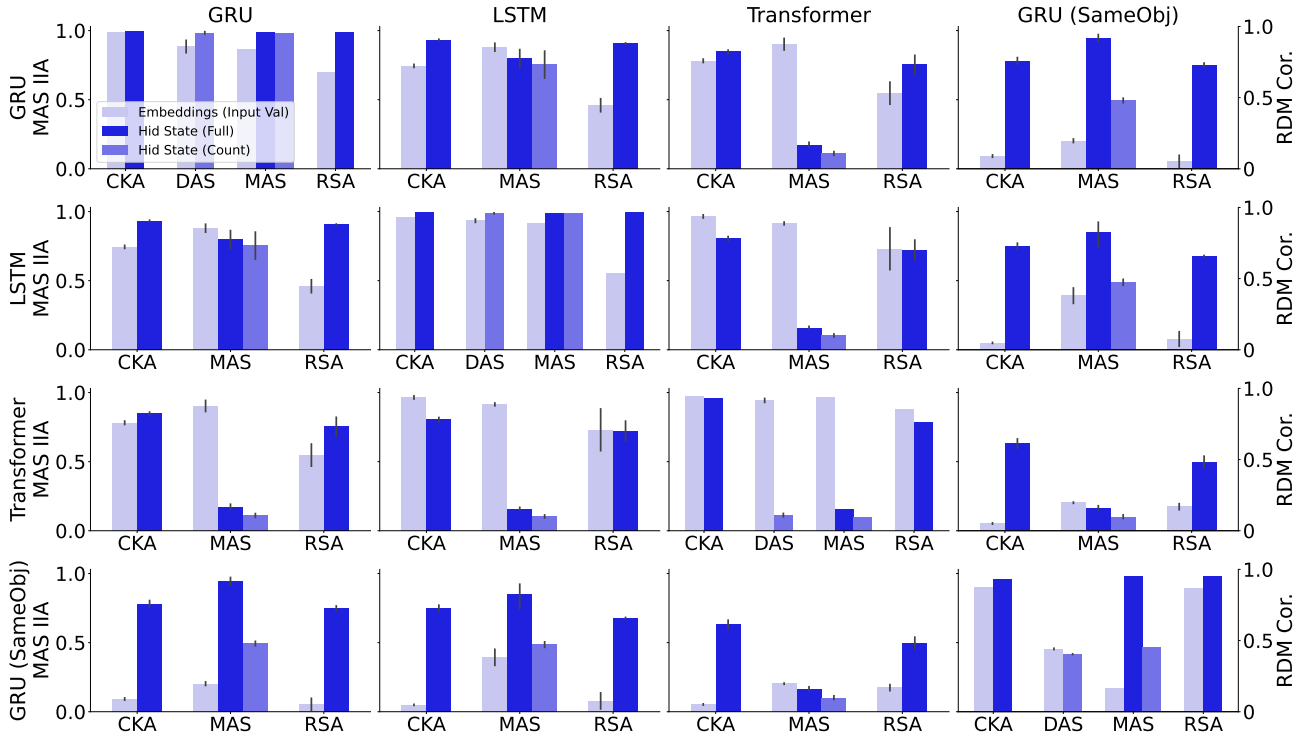


Figure 8: A performance comparison of MAS against RSA. The rows of panels show Model 1 whereas the columns represent the Model 2 in the context of the MAS diagram Figure 2. The different colors represent different activation layers within the models, and, in the case of MAS, the colors further distinguish which causal variables the analysis was conditioned upon.

A.1. Model Details

All artificial neural network models were implemented and trained using PyTorch (Paszke et al., 2019) on Nvidia Titan X GPUs. Unless otherwise stated, all models used an embedding and hidden state size of 48 dimensions. To make the token predictions, each model used a two layer multi-layer perceptron (MLP) with GELU nonlinearities, with a hidden layer size of 4 times the hidden state dimensionality with 50% dropout on the hidden layer. The GRU and LSTM model variants each consisted of a single recurrent cell followed by the output MLP. Unless otherwise stated, the transformer architecture consisted of two layers using Rotary positional encodings (Su et al., 2023). Each model variant used the same learning rate scheduler, which consisted of the original transformer (Vaswani et al., 2017) scheduling of warmup followed by decay. We used 100 warmup steps, a maximum learning rate of 0.001, a minimum of 1e-7, and a decay rate of 0.5. We used a batch size of 128, which caused each epoch to consist of 8 gradient update steps.

A.2. MAS (and Associated Variants) Training Details

For each rotation matrix training, we use 10000 intervention samples and 1000 samples for validation and testing. We uniformly sampled corresponding indices upon which to perform interventions, excluding the B, T, and E tokens in the numeric equivalence tasks from possible intervention sample indices. In the Arithmetic task, we used the comma token for Rem Ops and Cumu Val interventions. When intervening upon a state in the demo phase in the numeric equivalence tasks, we uniformly sample 0-3 steps to continue the demo phase before changing the phase by inserting the trigger token. We orthogonalize the matrices, Q_i , using PyTorch’s orthogonal parametrization with default settings. PyTorch creates the orthogonal matrix as the exponential of a skew symmetric matrix. We train the rotation matrices for 1000 epochs, with a batch size of 512 used for each model index pairing. We only perform experiments considering two models. Each gradient step uses the average gradient over batches of all i, j pairings. We select the checkpoint with the best validation performance for analysis. We use a learning rate of 0.003 and an Adam optimizer.

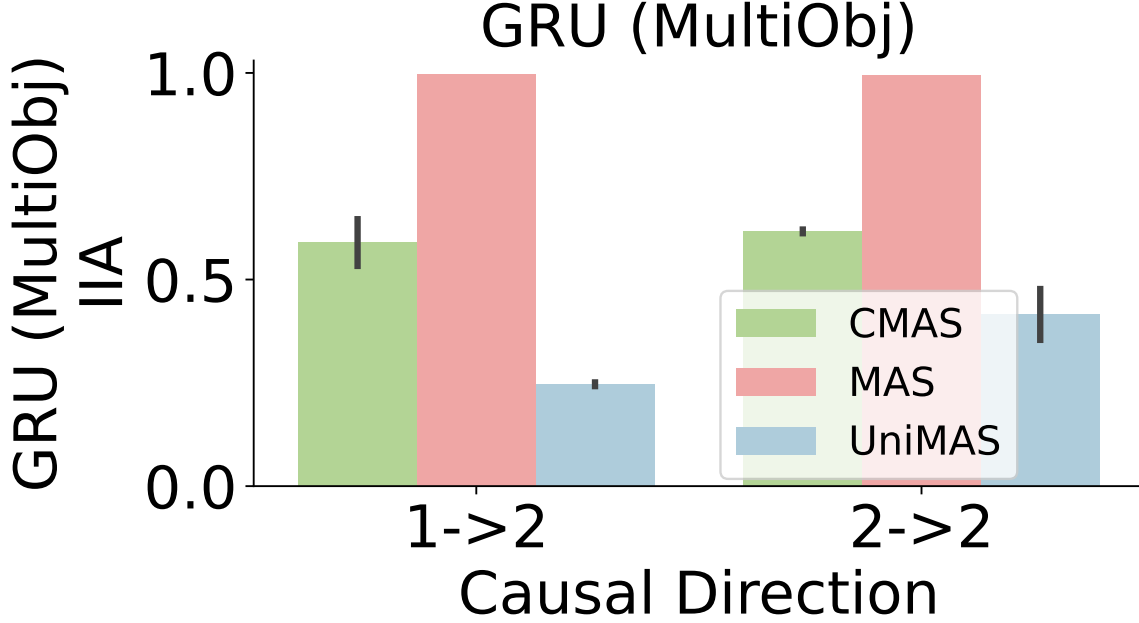


Figure 9: The IIAs in the causally untrained directions for CMAS on the Multi-Object GRU models on the Count variable. The x labels denote the intervention directions where the numbers 1 and 2 denote the model index and the arrow points from the source to the target model. UniMAS and MAS show a lower and upper bound on CMAS performance.

A.3. RSA Details

We performed RSA on a dataset of 15 sampled sequences for each object quantity ranging from 1-20 on the task that each model was trained on for each model. We first ran the models on their respective datasets to collect the latent representations. We then used each of these latent vectors as the sample representations in a matrix $M_k \in R^{N \times d_k}$ where k refers to the model index, N is the number of latent vectors ($N = 15 \times 20 = 300$ in our analyses), d_k is the dimensionality of a single latent vector for model k . We then calculated the sample correlation matrices for each model resulting in matrices $C_k \in R^{N \times N}$. Lastly we calculated the Spearman's Rank Correlation Coefficient between the matrices C_1 and C_2 as the RSA value (Zar, 2005; Kriegeskorte et al., 2008).